Journal of
Micro/Nanolithography,
MEMS, and MOEMS

Nanolithography.SPIEDigitalLibrary.org

Microfabricated water-immersible scanning mirror with a small form factor for handheld ultrasound and photoacoustic microscopy

Song Xu
Chih-Hsien Huang
Jun Zou

SPIE.

Microfabricated water-immersible scanning mirror with a small form factor for handheld ultrasound and photoacoustic microscopy

Song Xu, Chih-Hsien Huang, and Jun Zou*
Texas A&M University, Institute for Solid State Electronics, Electrical Engineering Department, Room 220A, Wisenbaker Engineering Building, College Station, Texas 77843-3128, United States

Abstract. Microscanning mirrors that can operate reliably under water are useful in both ultrasound and photoacoustic microscopic imaging, where fast scanning of focused high-frequency ultrasound beams is desired for pixel-by-pixel data acquisition. We report the development of a new microfabricated water-immersible scanning mirror with a small form factor. It consists of an optically and acoustically reflective mirror plate which is supported by two flexible polymer hinges and driven by an integrated electromagnetic microactuator. It can achieve 1-axis scanning of ± 12.1 deg at a resonant frequency of 250 Hz in air and 210 Hz in water, respectively. By optimizing the design and enhancing the fabrication with high-precision optical three-dimensional printing, the overall size of the scanning mirror module is less than 7 mm $\times$ 5 mm $\times$ 7 mm. The small form factor, large scanning angle, and high-resonant frequency of the new water-immersible scanning mirror make it suitable for building compact handheld imaging probes for *in vivo* high-speed and wide-field ultrasound and photoacoustic microscopy. [DOI: 10.1117/1.JMM.14.3.035004]

Keywords: water-immersible; scanning mirror; ultrasound; photoacoustic; microscopy.

Paper 15081 received May 16, 2015; accepted for publication Jul. 30, 2015; published online Sep. 4, 2015.

1 Introduction

Recently, ultrasound and photoacoustic microscopy have become useful high-resolution microscopic imaging techniques with a broad range of applications.[1–3] To conduct ultrasound and photoacoustic microscopy, a high-frequency ultrasound beam (and also a pulsed laser beam in the case of photoacoustic microscopy) is focused and mechanically scanned over the imaging target pixel-by-pixel to acquire the ultrasound data for image reconstruction. Usually, the mechanical scanning is performed with a 2-axis motor stage, which is often heavy, bulky, and slow, and is, therefore, mainly suitable for table-top operations. In the past few years, microelectromechanical systems (MEMS) scanning mirrors have been developed.[4–6] They have a much smaller form factor and much higher scanning speeds than the motor stages, which make them a good choice of scanning elements for developing compact imaging probes for handheld operations. However, current MEMS scanning mirrors are designed for free-space optical beam steering in air. They are not suitable for the underwater scanning operations required by ultrasound and photoacoustic microscopy, where water is used as the matching medium for the transmission of high-frequency ultrasound waves.

To address this issue, we have developed a water-immersible microscanning mirror, which can reliably operate in both air and water to provide fast scanning of both optical and high-frequency ultrasonic beams in water.[7] It has been used to enable high-speed and high-resolution photoacoustic microscopy to capture the fast-changing functional information of biological tissues.[8–10] However, due to the limitations in its design and construction, the water-immersible microscanning mirror has a large form factor which cannot be accommodated inside a compact probe for handheld imaging operations. In this paper, we report the development of a new 1-axis water-immersible microscanning mirror with a much smaller form factor. By optimizing the design and improving the fabrication by using high-resolution three-dimensional (3-D) printing, the overall size of the water-immersible microscanning mirror has been significantly reduced without any degradation in its scanning performance. This makes it suitable for building compact handheld imaging probes to conduct ultrasound and photoacoustic microscopy where the water-immersible scanning mirror can be used to provide the primary (fast)-axis scanning.

2 Design

Figure 1 shows the schematic design of the new water-immersible scanning mirror. A single-crystal silicon substrate coated with a thin aluminum layer is used as the reflective mirror plate. Silicon has a much higher acoustic impedance than water and provides high-acoustic reflectivity, while the aluminum coating forms a good optical reflection layer. The mirror plate has a rectangular shape to better fit the oval optical/ultrasound illumination spot. Compared with that of conventional microscanning mirrors, the mirror plate has a much larger size to provide a higher numerical aperture for ultrasound beam steering. This is improtant to ensure good acoustic sensitivity, especially when the ultrasound signals are weak. The mirror plate is supported by two microtorsion hinges separated by a spacer frame [Fig. 1(b)], which are made of high-strength biaxially oriented polyethylene terephthalate (BOPET) film. Its low stiffness and high fracture strain reduce the required driving

*Address all correspondence to: Jun Zou, E-mail: junzou@ece.tamu.edu

1932-5150/2015/$25.00

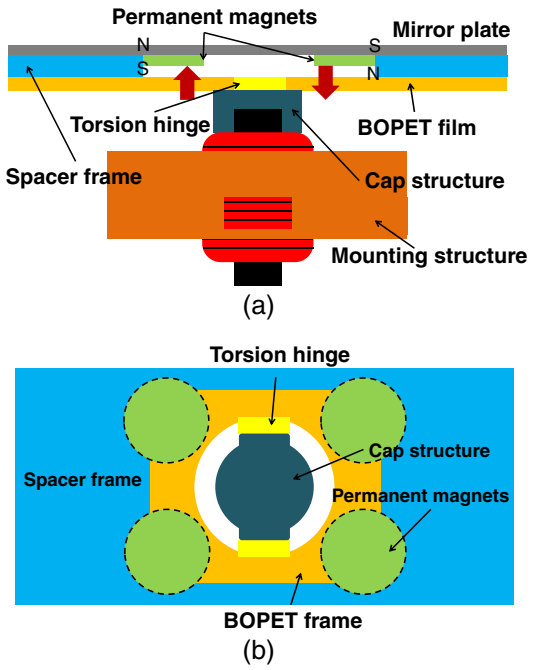

Fig. 1 Schematics of the water-immersible scanning mirror design: (a) side view and (b) top view with mirror plates removed.

force and avoid shock damage due to turbulence, especially for a larger mirror plate. The outer ends of the two torsion hinges are attached onto the spacer frame. Their inner ends are anchored onto the cap structure on the inductor coil housed in a supporting base, which also serves as the mounting structure of the scanning mirror. Both the hinges and magnets are buried underneath the mirror plate to minimize the overall dimensions of the mirror module.

Electromagnetic actuation was chosen as the driving mechanism. Compared with other microactuation mechanisms, such as electrostatic, piezoelectric, and thermal methods, electromagnetic actuation does not need a high voltage or electroheating,[11,12] and is, therefore, more suitable in a liquid environment. Compact electromagnetic actuation was achieved by combining a single inductor coil with two pairs of four rare-earth magnet discs attached onto the two ends of the mirror plate with opposite polarities. When the AC current flows through the inductor coil, the resultant magnetic field creates a torque on the magnets and vibrates the mirror plate around the two torsion hinges. To achieve significant reduction of the overall size of the mirror module, improvements were made over the previous design. First, instead of being placed adjacent to the mirror plate, the two torsion hinges are completely covered underneath it. Second, the inductor coil is used as the supporting structure of the mirror plate assembly. Third, the use of four magnets instead of two provides a stronger and more uniform magnetic field, which allows the use of a smaller inductor coil to drive the scanning mirror.

In ultrasound and photoacoustic microscopy, the optical and ultrasound signals are in the form of short pulses with a typical repetition rate of 10 to 100 kHz. To maintain a dense pixel formation, the vibration frequency of the scanning mirror should be 10 to 100 of Hz. A maximal scanning angle larger than 10 deg is desirable to provide a good field of view. The main design parameters of the scanning mirror

Table 1 Design parameters of the mirror.

Inductor		Permanent magnets	
Inductance	1 mH	Thickness	0.8 mm
		Diameter	3.125 mm
		Spacing	3 mm × 4 mm
Mirror plate		Supporting hinge	
Length	7 mm	Length	0.75 mm
Width	5 mm	Width	5 mm
Thickness	0.3 mm	Thickness	0.3 mm

are listed in Table 1. Based on these design parameters, a preliminary mechanical analysis was conducted to provide a first-order estimation of the scanning performances (e.g., scanning angle, resonant frequency, and driving current).[13] The magnetic force (F) generated between the permanent magnet discs and the inductor coil can be determined by

$$F = V \times M_s \times \frac{\partial H}{\partial z}, \tag{1}$$

where V is the total volume of two permanent magnetic discs, M_s is the effective magnetization of the two magnet discs on each side, and H is the magnetic field intensity generated by the inductor. The torque T_{mag} generated by the magnetic force and the resulting rotation angle (ϕ) can be determined by

$$T_{\text{mag}} = F \times L', \tag{2}$$

$$\phi = \frac{TL}{JG}, \tag{3}$$

where L, J, and G are the length, torsional moment of inertia, and shear modulus of elasticity of the torsion hinges, respectively, and L' is the work distance between the magnetic force (F) and the torsion hinges. Assuming the torsion hinge has a rectangular cross-section, the torsion moment of inertia (J) can be determined by

$$J = wt^3\left[\frac{16}{3} - 3.36\frac{t}{w}\left(1 - \frac{t^4}{12w^4}\right)\right], \tag{4}$$

where w is the width and t is the thickness of the torsion hinge. The resonant frequency in air (f_{r_air}) can be estimated by

$$f_{r\_\text{air}} = \frac{1}{2\pi}\sqrt{\frac{K^\star}{m}}, \tag{5}$$

where $K^\star$ is the torsional force constant of the BOPET hinges and m is the overall effective mass of the mirror plate assembly. Due to the small movement of the mirror plate during scanning, the damping from the air can be neglected.

Table 2 Estimated resonance frequencies.

f_{r_air}	263.42 Hz
f_{r_water}	215.73 Hz

When the scanning mirror is immersed in water, the resonant frequency (f_{r_water}) can be estimated by

$$f_{r\_water} = f_{r\_air}\sqrt{1+\frac{3\pi\rho b}{2\rho_m t'}\Gamma_t(\kappa)}^{-1}, \quad (6)$$

where ρ is the density of water, ρ_m and b are the effective density and width of the mirror plate assembly, $\Gamma_t(\kappa)$ is the normalized hydrodynamic load (i.e., the "hydrodynamic function"[14]), which depends on the normalized mode order (κ), by

$$\Gamma_t(\kappa) = \frac{1}{16}\left(\frac{1+0.37922\kappa+0.072912\kappa^2}{1+0.37922\kappa+0.088056\kappa^2+0.010737\kappa^3}\right), \quad (7)$$

and κ is determined by the mode number n ($n=1$ for first-order resonance) and cantilever length L and width b[15]

$$\kappa = \frac{\pi}{2}(2n-1)\frac{b}{L}. \quad (8)$$

Since the water tank (60-cm long, 30-cm wide, and 20-cm deep) is much larger than mirror module (7 mm × 5 mm × 7 mm), the boundary effect of the water tank on the damping is negligible. Based on Eqs. (1)–(8), the estimated resonant frequencies of the scanning mirror in both air and water are listed in Table 2.

3 Fabrication and Assembly

The fabrication of the scanning mirror starts with the preparation of the reflective mirror plate. A 300 μm thick single-crystalline silicon wafer was coated with a 150nm thick aluminum layer by using electron-beam evaporation (PVD 75 Ebeam Evaporator, Lesker). After this, it was cut into multiple 7 mm × 5 mm pieces using an automatic dicing machine (1006A, Micro Automation), which will be used as the reflective mirror plate. The torsion hinges, spacer frame, and inductor cap were made by using a laser cutting machine (PLS6.75, Universal Laser System). The torsion hinges were cut out from a 75 μm thick BOPEF film, and the spacer frame and inductor cap were cut out from a 1-mm thick acrylic sheet. Because of its complex 3-D shape, the inductor housing (with two mounting holes inside) were fabricated by using a high-resolution optical 3-D printer (Perfactory® Micro DDP, Envisiontec) with a maximal resolution of 30 μm.

After all the components were fabricated, the silicon mirror plate, spacer frame, permanent magnetic discs (D101-N52, K&J Magnetics), and BOPET torsional hinges were first assembled and bonded together with silicone rubber adhesive (RTV 108, Momentive Performance Materials) [Fig. 2(a)]. Second, one end of the magnetic core of the inductor coil (70F103AI-RC, BOURNS) was polished into a flat surface, followed by the mounting and bonding of the inductor cap. Next, the inner ends of the two torsional hinges were bonded onto the inductor cap. In the last step, two electrical wires were connected to the inductor coil and insulated with silicone rubber adhesive. Figs. 2(e) and 2(f) show a completely assembled scanning module. It has an overall length, width, and thickness of 7, 5, and 7 mm, respectively, which is much smaller than our previous scanning mirror module with an overall size of 15 mm × 15 mm × 15 mm.[7]

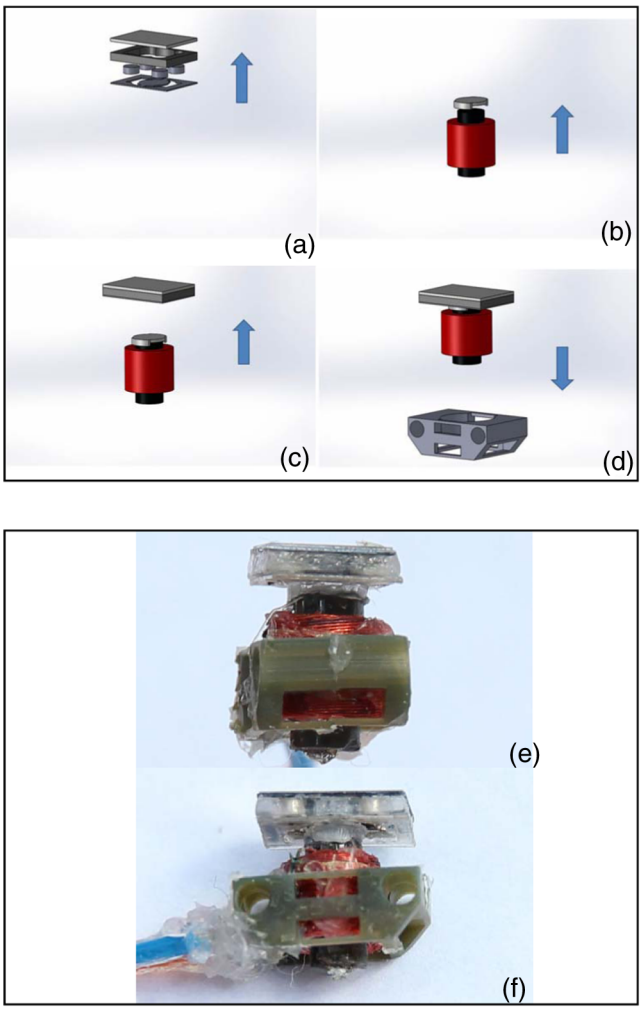

Fig. 2 (a)–(d) Illustration of the scanning mirror assembly process and (e)–(f) right-side and front-side views of a fully assembled scanning mirror module.

4 Characterization

The scanning angle ϕ and resonance frequency f_r of the scanning mirror were characterized in air and water by using a laser tracing method (Fig. 3). During the characterization, the scanning mirror was mounted on the bottom of a water tank. A ruler was placed 35 mm away from the center of the mirror plate. The laser beam from a laser pointer was projected onto the mirror plate with an incident angle of 45 deg and reflected onto the ruler. The scanning angle was calculated based on the trace of the laser beam on the ruler. To determine the resonance frequency, AC driving currents with the same amplitude but different frequencies were applied. The resonance frequency is defined as the frequency of the AC driving current when the scanning angle

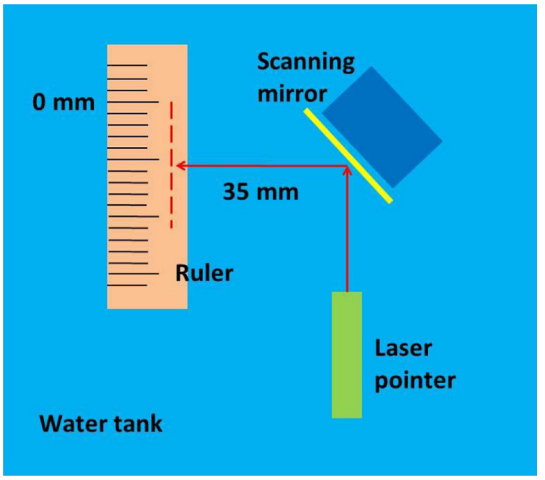

Fig. 3 Laser tracing setup for the characterization of the scanning angle and resonant frequency.

reaches its maximum. Figure 4(a) shows the scanning angles at different frequencies both in air and in water. The amplitude of the AC driving currents is 90 mA in air and 97 mA in water, respectively. Due to the dynamic damping in water, the resonance frequency drops from 250 Hz in air to 210 Hz in water, which are close to the estimated values. Figures 4(b)–4(e) show the average values and standard deviations of the optical tilting angles (based on five measurements) as a function of the amplitude of the AC currents when the scanning mirror was driven at its resonant frequency in air and water, respectively. In water, as the current increasing from 20 to 120 mA, the optical tilting angle increases linearly from 4 deg to 12.5 deg. On the other hand, as the current decreases from 120 to 20 mA, the linearity can also be observed. In air, at low current, the optical tilting angle also varies linearly with respect to the AC current. However, at high current, linearity is distorted a little because the tilting angle is so large that the BOPET hinge

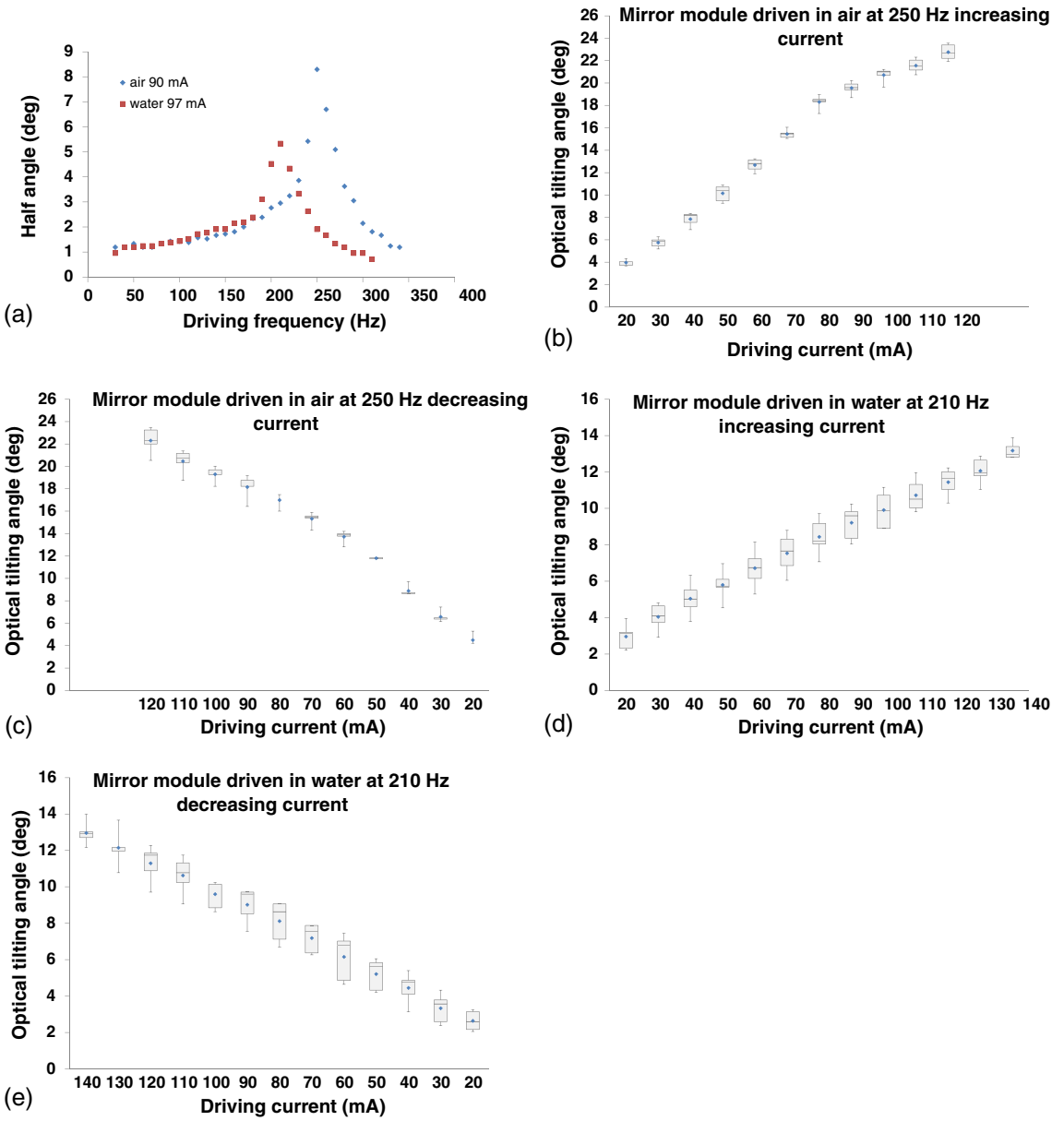

Fig. 4 (a) Resonant frequency test results and (b)–(e) optical tilting angle test results.

can no longer hold its mechanical property. Since the tilting angles required in ultrasound and photoacoustic scanning are usually smaller than nonlinear region values, it is safe to draw a conclusion that the optical tilting angle increases linearly with the amplitude of the AC driving currents. In addition, a thermal conductivity and reliability test was also performed when the scanning mirror was immersed in water at 25°C. A thermal couple probe was put in direct touch with the inductor coil to monitor the change of its temperature. The scanning mirror was driven at 210 Hz with an AC current of 230 mA. The temperature of the inductor coil stayed constantly at 31°C. After being driven over 10 million cycles, no noticeable degradation in the scanning performance was observed.

5 Ultrasound Imaging Experiment

Using the water-immersible scanning mirror to steer a focused ultrasound beam in water, pulse-echo ultrasound microscopy of an optical-fiber target was successfully demonstrated. The imaging setup (Fig. 5) includes a water tank, a high-frequency (25 MHz) focused transducer with a focal length of 50.4 mm (V324-SM-F2.00IN-PTF, Olympus), the water-immersible scanning mirror, and a piece of 0.9-mm pencil lead as the imaging target. The scanning mirror is placed 28 mm away from the transducer at an angle of 45 deg. The pencil lead is placed 32 mm away from the center of the mirror plate, such that they are located in the focal zone of the ultrasound transducer. The ultrasound transducer is connected to a pulser/receiver system (5072PR, Olympus) and an oscilloscope (TDX 2014B, Tektronix). The pulses' repetition rate and pulse width were set to be 5 kHz and 1 s, respectively. A data acquisition (DAQ) card (PCI 6251, National Instruments) and a custom-built current amplifier array were used to provide DC currents to drive the scanning mirror from −350 to 350 mA with a 7 mA increment. This forms 100 scanning steps, corresponding to a scanning area of 3 mm. The peak-to-peak voltage of the received ultrasound signals were measured and averaged 128 times. To automate the scanning and data acquisition process, a Labview (National Instruments) program was developed to control the DAQ card and the oscilloscope. Figure 6 shows the normalized averaged peak-to-peak voltages as a function of the lateral and vertical scanning location. The target width is 1.08 mm in the ultrasound image, which agreed well with the actual pencil lead width. There are two hot spots in the ultrasound image. One illustrates the upper water-target interface and the other one illustrates the bottom target-water interface. The space between these two surfaces denotes the target.

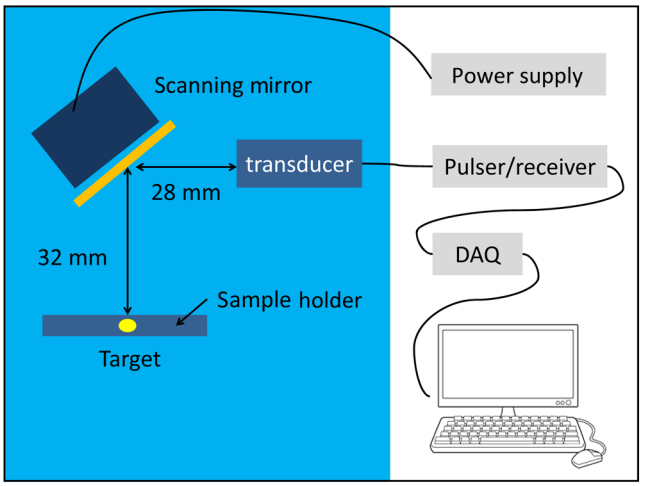

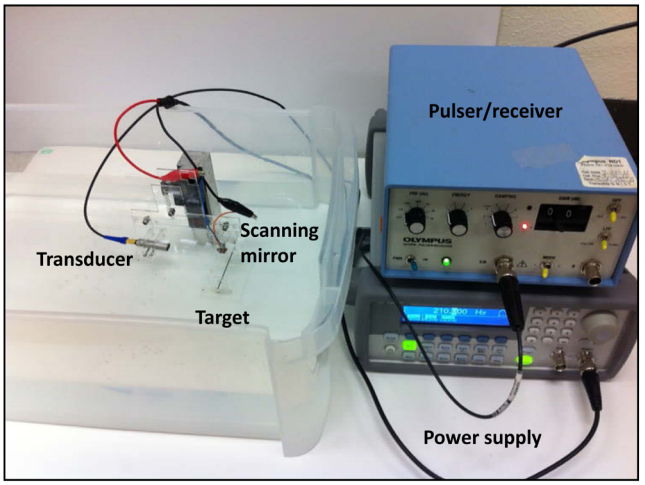

Fig. 5 The pulse/echo ultrasound microscopic imaging setup.

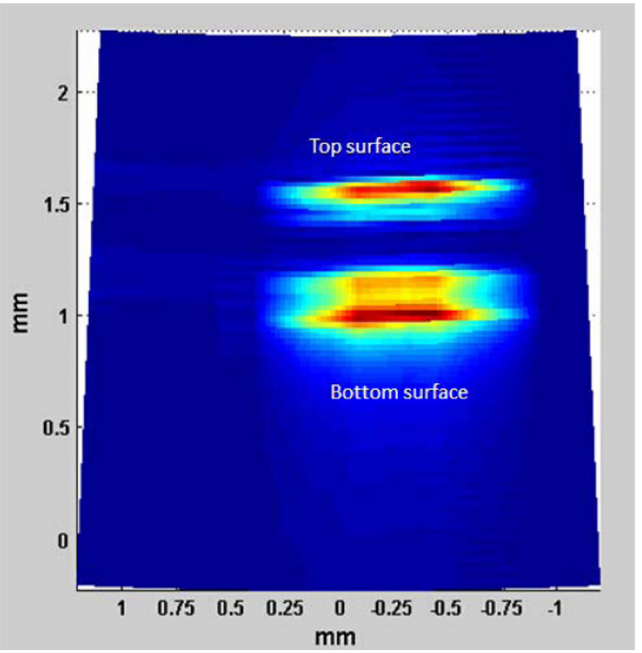

Fig. 6 Ultrasound B-scan result.

6 Conclusion

In conclusion, we have demonstrated a new water-immersible scanning mirror with a small form factor. Compared with its predecessors, a significant size reduction of the entire scanning mirror module has been achieved without sacrificing the scanning range and speed. This is made possible with design optimization and a seamless integration of conventional microfabrication processes with new 3-D printing technologies. Future work will be focused on its application in the development of new handheld ultrasound and photoacoustic imaging modalities.

Acknowledgments

This work was supported in part by a grant from the National Science Foundation (IDBR-1255921) and a grant from the March of Dimes Foundation under Prematurity Research Center at Washington University in St. Louis. The authors would like thank Prof. Lihong V. Wang and Dr. Konstantin Maslov for helpful discussions.

References

1. M. Xu and L. V. Wang, "Photoacoustic imaging in biomedicine," *Rev. Sci. Instrum.* **77**(4), 041101 (2006).
2. C. Zhang et al., "In vivo photoacoustic microscopy with 7.6-μm axial resolution using a commercial 125-mhz ultrasonic transducer," *J. Biomed. Opt.* **17**(11), 116016 (2012).
3. L. Song et al., "Ultrasound-array-based real-time photoacoustic microscopy of human pulsatile dynamics in vivo," *J. Biomed. Opt.* **15**(2), 021303 (2010).
4. P. Deng and W. Ma, "Nonlinearity investigation of the MEMS scanning mirror with electrostatic comb drive," in *2014 9th IEEE Int. Conf. on Nano/Micro Engineered and Molecular Systems (NEMS)*, pp. 212–215, IEEE (2014).
5. T. Naono et al., "A large-scan-angle piezoelectric MEMS optical scanner actuated by a Nb-doped PZT thin film," *J. Micromech. Microeng.* **24**(1), 015010 (2014).
6. G. Brown et al., "A two-axis hybrid mems scanner incorporating electrothermal and electrostatic actuators," in *Proc. IEEE Int. Conf. Opt. MEMS Nanophoton*, pp. 115–116 (2010).
7. C.-H. Huang et al., "A water-immersible 2-axis scanning mirror microsystem for ultrasound andha photoacoustic microscopic imaging applications," *Microsyst. Technol.* **19**(4), 577–582 (2013).
8. J. Yao et al., "Wide-field fast-scanning photoacoustic microscopy based on a water-immersible MEMS scanning mirror," *J. Biomed. Opt.* **17**(8), 080505 (2012).
9. J. Yao et al., "High-speed label-free functional photoacoustic microscopy of mouse brain in action," *Nat. Methods* **12**(5), 407–410 (2015).
10. C. Martel et al., "Photoacoustic lymphatic imaging with high spatial-temporal resolution," *J. Biomed. Opt.* **19**(11), 116009 (2014).
11. I.-J. Cho and E. Yoon, "A low-voltage three-axis electromagnetically actuated micromirror for fine alignment among optical devices," *J. Micromech. Microeng.* **19**(8), 085007 (2009).
12. K. H. Kim et al., "Two-axis magnetically-driven MEMS scanning catheter for endoscopic high-speed optical coherence tomography," *Opt. Express* **15**(26), 18130–18140 (2007).
13. Y. Zhang et al., "Design and analysis of the micromechanical structure for an electromagnetic bistable RF MEMS switch," in *Asia-Pacific Conf. Proc. Microwave Conf. Proc. (APMC 2005)*, Vol. 1, p. 4, IEEE (2005).
14. F.-J. Elmer and M. Dreier, "Eigenfrequencies of a rectangular atomic force microscope cantilever in a medium," *J. Appl. Phys.* **81**(12), 7709–7714 (1997).
15. C. A. Van Eysden and J. E. Sader, "Resonant frequencies of a rectangular cantilever beam immersed in a fluid," *J. Appl. Phys.* **100**(11), 114916 (2006).

Song Xu received his BS degree in optical and electrical engineering from Huazhong University of Science and Technology, China, in 2012. Currently, he is pursuing his PhD in the Department of Electrical and Computer Engineering at Texas A&M University. His current research involves building MEMS scanning mirrors for SAM and PAM and ultrasound image reconstruction.

Chih-Hsien Huang received his BS and MS degrees in electrical engineering from National Cheng Kung University, Tainan, Taiwan, in 2003 and 2005, respectively. From 2005 to 2010, he was with Industrial Technology Research Institute, Tainan, Taiwan, where he developed various feedback control methodologies for LED backlight system. In 2010, he joined the Department of Electrical and Computer Engineering at Texas A&M. His research interest is focused on MEMS based scanning transducer for acoustic imaging applications.

Jun Zou received his PhD degree in electrical engineering from the University of Illinois at Urbana-Champaign in 2002. In 2004, he joined in the Department of Electrical and Computer Engineering at Texas A&M University, where he is currently an associate professor. His current research interests lie in the development of micro- and nano-optoelectromechanical devices and systems for biomedical imaging and sensing applications.